Radka Keslerová; Karel Kozel

Steady and unsteady 2D numerical solution of generalized Newtonian fluids flow

In: Jan Brandts and J. Chleboun and Sergej Korotov and Karel Segeth and J. Šístek and Tomáš Vejchodský (eds.): Applications of Mathematics 2012, In honor of the 60th birthday of Michal Křížek, Proceedings. Prague, May 2-5, 2012. Institute of Mathematics AS CR, Prague, 2012. pp. 117–126.

Persistent URL: http://dml.cz/dmlcz/702898

Conference Applications of Mathematics 2012
in honor of the 60th birthday of Michal Křížek.
Institute of Mathematics AS CR, Prague 2012

STEADY AND UNSTEADY 2D NUMERICAL SOLUTION OF GENERALIZED NEWTONIAN FLUIDS FLOW

Radka Keslerová, Karel Kozel

Czech Technical University, Faculty of Mechanical Engineering
Department of Technical Mathematics
Karlovo nám. 13, 121 35 Prague, Czech Republic
keslerov@marian.fsik.cvut.cz, Karel.Kozel@fs.cvut.cz

Abstract

This article presents the numerical solution of laminar incompressible viscous flow in a branching channel for generalized Newtonian fluids. The governing system of equations is based on the system of balance laws for mass and momentum. The generalized Newtonian fluids differ through choice of a viscosity function. A power-law model with different values of power-law index is used. Numerical solution of the described models is based on cell-centered finite volume method using explicit Runge–Kutta time integration. The unsteady system of equations with steady boundary conditions is solved by finite volume method. Steady state solution is achieved for $t \to \infty$. In this case the artificial compressibility method can be applied. For the time integration an explicit multistage Runge–Kutta method of the second order of accuracy in the time is used. In the case of unsteady computation two numerical methods are considered, artificial compressibility method and dual-time stepping method. The flow is modelled in a bounded computational domain. Numerical results obtained by this method are presented and compared.

1. Introduction

Generalized Newtonian fluids can be subdivided according to the viscosity behaviour. For Newtonian fluids the viscosity is constant and is independent of the applied shear stress (examples: water, kerosene etc). Shear thinning fluids are characterized by decreasing viscosity with increasing shear rate (ketchup, honey, blood etc). Shear thickening fluids are characterized by increasing viscosity with increasing shear rate (wet sand etc.). For more details see e.g. [1].

2. Mathematical model

The governing system of equations is the system of balance laws of mass and momentum for incompressible fluids [2]:

$$\operatorname{div} \boldsymbol{u} = 0 \tag{1}$$

$$\rho\frac{\partial \boldsymbol{u}}{\partial t} + \rho(\boldsymbol{u}.\nabla)\boldsymbol{u} = -\nabla P + \text{div } \mathbf{T} \tag{2}$$

where P is pressure, ρ is constant density, $\boldsymbol{u}$ is velocity vector. The symbol $\mathbf{T}$ represents the stress tensor.

The commonly used model corresponding to Newtonian fluid is Newtonian model:

$$\mathbf{T} = 2\mu\ \mathbf{D} \tag{3}$$

where μ is dynamic viscosity and tensor $\mathbf{D}$ is symmetric part of the velocity gradient defined by the relation

$$\mathbf{D} = \frac{1}{2}(\nabla\boldsymbol{u} + \nabla\boldsymbol{u}^T) = \frac{1}{2}\begin{pmatrix} 2u_x & u_y + v_x \\ u_y + v_x & 2v_y \end{pmatrix} \tag{4}$$

This model could be generalized to take into account shear thinning and shear thickening behaviour

$$\mathbf{T} = 2\mu_\epsilon\mu\ \mathbf{D}. \tag{5}$$

For this case the viscosity μ is no more constant, but is defined by viscosity function $\mu(\dot\gamma)$ according to the power-law model, [7]

$$\mu = \mu(\dot\gamma) = \left(\sqrt{\text{tr}\mathbf{D}^2}\right)^r, \tag{6}$$

where $\dot\gamma = \sqrt{\text{tr}\mathbf{D}^2}$ is shear rate, μ_ϵ is a constant, e.g. the dynamic viscosity for Newtonian fluid. The symbol tr $\mathbf{D}^2$ denotes trace of the tensor $\mathbf{D}^2$. The exponent r is the power-law index. This model includes Newtonian fluids as a special case ($r = 0$). For $r > 0$ the power-law fluid is shear thickening, while for $r < 0$ it is shear thinning.

3. Numerical solution

3.1. Steady case

In this case the artificial compressibility method can be applied. It means that the continuity equation is completed by term $\frac{1}{\beta^2}p_t$. For more details see e.g. [3]. This yields in the conservative form (non-dimensional):

$$\tilde{R}_\beta W_t + F^c_x + G^c_y = \frac{1}{\text{Re}}(F^v_x + G^v_y), \tag{7}$$

$$\tilde{R}_\beta = \text{diag}(\frac{1}{\beta^2}, 1, 1), \quad \beta \in \mathbf{R}^+ \tag{8}$$

where W is vector of unknowns, $p = P/\rho$ is pressure, u, v are velocity components, F^c, G^c are inviscid fluxes and F^v, G^v are viscous fluxes defined as

$$W = \begin{pmatrix} p \\ u \\ v \end{pmatrix},\ F^c = \begin{pmatrix} u \\ u^2 + p \\ uv \end{pmatrix},\ G^c = \begin{pmatrix} v \\ uv \\ v^2 + p \end{pmatrix}, \tag{9}$$

$$F^v = \begin{pmatrix} 0 \\ 2\mu(\dot\gamma)u_x \\ \mu(\dot\gamma)(v_x+u_y) \end{pmatrix}, \quad G^v = \begin{pmatrix} 0 \\ \mu(\dot\gamma)(u_y+v_x) \\ 2\mu(\dot\gamma)v_y \end{pmatrix} \tag{10}$$

The symbol Re denotes Reynolds number defined by the expression

$$\mathrm{Re} = \frac{\rho U L}{\mu_\epsilon}, \tag{11}$$

where U, L are reference velocity and length, μ_ϵ is dynamic Newtonian viscosity and ρ is constant density. The parameter β has dimension of a speed and denotes the artificial speed of sound. In the case of non-dimensional equations, β is then divided by a reference velocity U. This is usually an upstream velocity, which does not significantly differ from the maximum velocity in the flow field. Hence, in the case of non-dimensional equations, $\beta = 1$ is used in the presented steady numerical simulations.

Equation (7) is discretized in space by the finite volume method (see [5]) and the arising system of ODEs is integrated in time by the explicit multistage Runge-Kutta scheme (see [4], [9]):

$$\begin{aligned} W_i^n &= W_i^{(0)} \\ W_i^{(s)} &= W_i^{(0)} - \alpha_{s-1}\Delta t \mathcal{R}(W)_i^{(s-1)} \\ W_i^{n+1} &= W_i^{(M)} \qquad\qquad s = 1, \ldots, M, \end{aligned} \tag{12}$$

where $M = 3$, $\alpha_0 = \alpha_1 = 0.5, \alpha_2 = 1.0$, the steady residual $\mathcal{R}(W)_i$ is defined by finite volume method as

$$\mathcal{R}(W)_i = \frac{1}{\mu_i}\sum_{k=1}^{4}\left[\left(\overline{F}_k^c - \frac{1}{\mathrm{Re}}\overline{F}_k^v\right)\Delta y_k - \left(\overline{G}_k^c - \frac{1}{\mathrm{Re}}\overline{G}_k^v\right)\Delta x_k\right], \tag{13}$$

where μ_i is the volume of the finite volume cell, $\mu_i = \int\int_{C_i} dx\, dy$. The symbols $\overline{F}_k^c, \overline{G}_k^c$ and $\overline{F}_k^v, \overline{G}_k^v$ denote the numerical approximation of the inviscid and viscous physical fluxes. The symbols Δx_k and Δy_k respectively are lengths of the kth-edge of the cell C_i in the x and y direction resp. The symbol Re is Reynolds number defined by (11). The mesh in the considered domain is assumed structured, the finite volume cells are quadrilateral.

The multistage Runge–Kutta scheme (12) is conditionally stable. The time step is chosen to satisfy the CFL conditions

$$\Delta t \le \min_{i,k} \frac{\mathrm{CFL}\ \mu_i}{\rho_A \Delta y_k + \rho_B \Delta x_k + \frac{2}{\mathrm{Re}}\mu(\dot\gamma)\left(\frac{(\Delta x_k)^2+(\Delta y_k)^2}{\mu_i}\right)} \tag{14}$$

index k describes the index of edges corresponding to the finite volume cell C_i. The volume of this cell is μ_i. The symbol CFL is so called Courant-Friedrichs-Lewy number. The Re is Reynolds number defined by (11) and $\mu(\dot\gamma)$ is defined by (6).

The global behaviour of the solution during the computational process is followed by the L^2 norm of the steady residuum. It is given by

$$\|\mathrm{Res}(W)^n\|_{L^2} = \sqrt{\sum_i \left(\frac{W_i^{n+1} - W_i^n}{\Delta t}\right)^2} \tag{15}$$

where $\mathrm{Res}(W)^n$ stands for a vector formed by the collection of $\mathrm{Res}(W)_i^n, \forall i$. The decadic logarithm of $\|\mathrm{Res}(W)^n\|_{L^2}$ is plotted in graphs presenting convergence history of simulation.

3.1.1. Steady boundary conditions

The flow is modelled in a bounded computational domain where a boundary is divided into three mutually disjoint parts: a solid wall, an outlet and an inlet. At the inlet Dirichlet boundary condition for velocity vector is used and for a pressure Neumann boundary condition is used. At the outlet the pressure value is given and for the velocity vector Neumann boundary condition is used. The homogenous Dirichlet boundary condition for the velocity vector is used on the wall. For the pressure Neumann boundary condition is considered.

Remark

The problem is to numerically solve Navier–Stokes equations for incompressible flows. Mathematical theory is possible to use for flow in one type of channel (steady) for one or more outputs where existence and unicity of the solution is proved (see [10], [11]).

3.2. Unsteady computation

Two approaches are used for numerical solution of unsteady flows. First, the artificial compressibility method is applied. In this case the artificial compressibility parameter β is set to be a big positive number, ideally $\beta \to \infty$. $\beta = 10$ is used in presented unsteady numerical simulations. In the second aproach dual-time stepping method is used.

The artificial compressibility approach used for unsteady incompressible flows is modifying the system of equations by adding an unsteady term to the continuity equation in the same way as for steady case.

The principle of dual-time stepping method is following. The artificial time τ is introduced and the artificial compressibility method in the artificial time is applied. The system of Navier-Stokes equations is extended to unsteady flows by adding artificial time derivatives $\partial W/\partial\tau$ to all equations, for more details see [8], [6]

$$\tilde{R}_\beta W_\tau + \tilde{R} W_t + F_x^c + G_y^c = F_x^v + G_y^v, \tag{16}$$

$$\tilde{R} = \mathrm{diag}(0, 1, 1), \quad \tilde{R}_\beta = \mathrm{diag}(\frac{1}{\beta^2}, 1, 1). \tag{17}$$

The vector of the variables W, the inviscid fluxes F^c, G^c and the viscous fluxes F^v, G^v are given by (9).

The derivatives with respect to the real time t are discretized using a three-point backward formula, it defines the form of unsteady residual

$$\tilde{R}_\beta \frac{W^{l+1} - W^l}{\Delta\tau} = -\tilde{R}\frac{3W^{l+1} - 4W^n + W^{n-1}}{2\Delta t} - \mathrm{Res}(W)^l = -\overline{\mathrm{Res}}(W)^{l+1}, \qquad (18)$$

where $\Delta t = t^{n+1} - t^n$ and $\mathrm{Res}(W)$ is the steady residual defined as for steady computation, see (13). The symbol $\overline{\mathrm{Res}}(W)$ denotes unsteady residual. The superscript n denotes the real time index and the index l is associated with the pseudo-time. The integration in pseudo-time can be carried out by explicit multistage Runge–Kutta scheme. The dual-time step $\Delta\tau$ is estimated using (14). The dual-time step is limited so that $\Delta\tau \leq 2\Delta t/3$.

The solution procedure is based on the assumption that the numerical solution at real time t^n is known. Setting $W_i^l = W_i^n, \forall i$, the iteration in l using explicit Runge-Kutta method are performed until the condition

$$\|\overline{\mathrm{Res}}(W)^l\|_{\mathrm{L}^2} = \sqrt{\sum_i \left(\frac{W_i^{l+1} - W_i^l}{\Delta\tau}\right)^2} \leq \epsilon \qquad (19)$$

is satisfied for a chosen small positive number ϵ. The symbol $\overline{\mathrm{Res}}(W)^l$ stands for the vector formed by the collection of $\overline{\mathrm{Res}}(W)_i^l, \forall i$. Once the condition (19) is satisfied for a particular l, one sets $W_i^{n+1} = W_i^{l+1}, \forall i$. Then the index representing real-time level can be shifted one up. History of the convergence of unsteady residual in dual time from t^n to t^{n+1} is plotted in decadic logarithm.

3.2.1. Unsteady boundary condition

The unsteady boundary conditions are defined as follows. In the inlet, in the solid wall and in one of the outlet part the steady boundary conditions are prescribed. In the second outlet part new boundary condition is defined. For the velocity Neumann boundary condition is used. The pressure value is prescribed by the function

$$p_{21} = \frac{1}{4}\left(1 + \frac{1}{2}\sin(\omega t)\right), \qquad (20)$$

where ω is the angular velocity defined as $\omega = 2\pi f$, where f is a frequency.

4. Numerical results

4.1. Steady numerical results

In this section the steady numerical results of two dimensional incompressible laminar viscous flows for generalized Newtonian fluids are presented. The different values of the power-law index were used. Reynolds number is 400.

In Figure 1 and 2 velocity isolines and histories of the convergence are presented. One of the main differences between Newtonian and non-Newtonian fluids flow is in

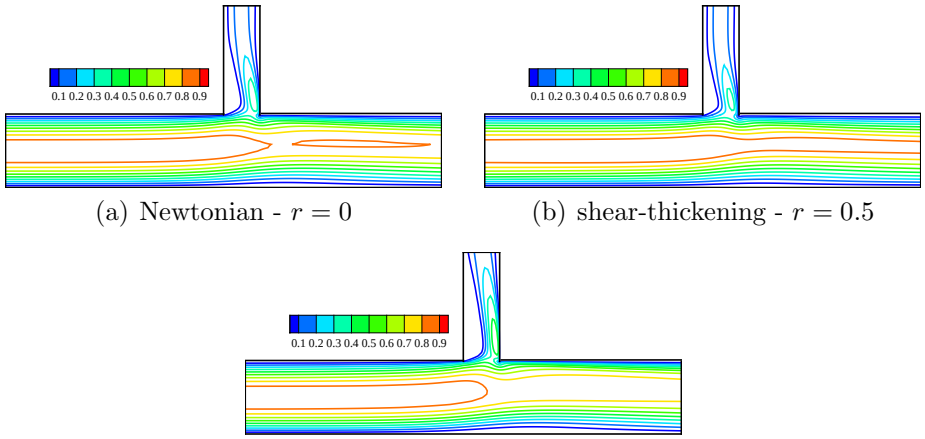

(a) Newtonian - $r = 0$ (b) shear-thickening - $r = 0.5$

(c) shear-thinning - $r = -0.5$

Figure 1: Velocity isolines of steady flows for generalized Newtonian fluids.

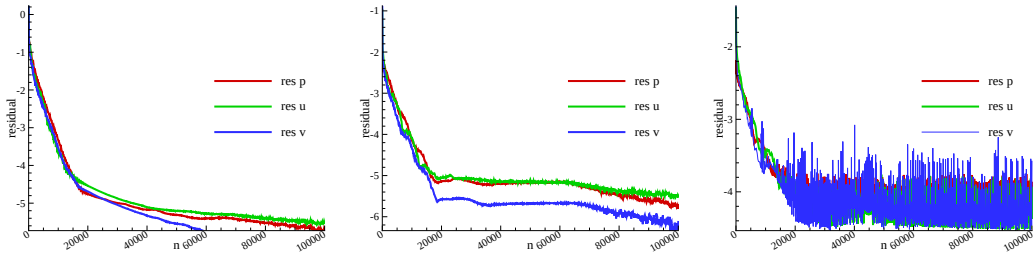

Figure 2: History of the convergence of steady flows for generalized Newtonian fluids.

the size of the separation region. This is in the place where the channel is branched. From Figures 1, the separation region is the smallest for shear thickening fluids and the biggest separation region is for the shear thinning fluids.

In Figure 3 nondimensional axial velocity profile for steady fully developed flow of generalized Newtonian. In these figures the small channel is sketched. The line (inside the domain) marks the position where the cuts for the velocity profile were done.

4.2. Unsteady numerical results

In this section two dimensional unsteady numerical results for generalized Newtonian flow through the branching channel are presented. The used unsteady methods are the artificial compressibility method and the dual-time stepping method with artificial compressibility coefficient $\beta = 10$. In the branch (going up) the pressure is prescribed by pressure function (20) with two frequencies f, 2 and 20. In Figure 4 and 5 numerical results for artificial compressibility method are presented. In the Figure 4 frequency is 2 and in the Figure 5 frequency is 20. First pictures show

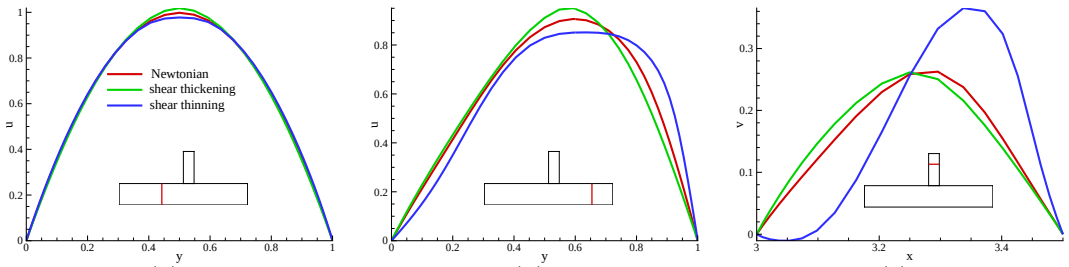

Figure 3: Nondimensional velocity profile for steady fully developed flow of generalized Newtonian fluids in the branching channel.

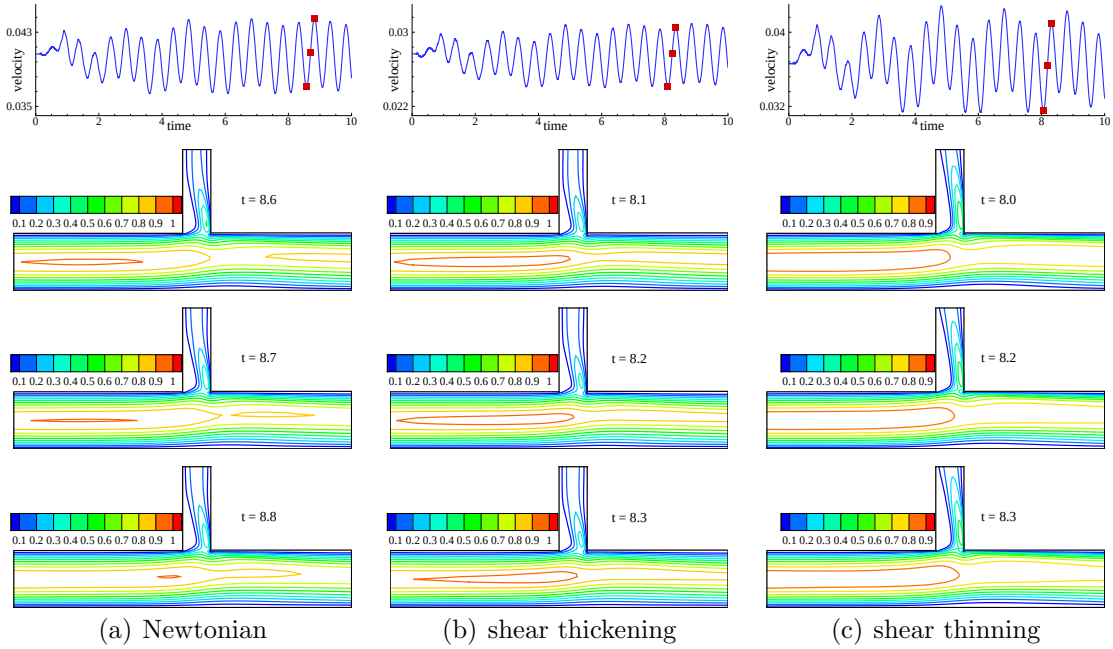

Figure 4: The graphs of the velocity as the function of time and velocity isolines of unsteady flow of generalized Newtonian fluids by artificial compressibility method (frequency is 2).

graphs of velocity. The square symbols mark positions in time of the snapshots shown in next three pictures during one period.

As initial data the numerical solution of steady fully developed flow of generalized Newtonian fluid in the branching channel was used. Reynolds number is 400.

Next used method is the dual-time stepping method. As in previous method three types of fluids were considered: Newtonian, shear thickening and shear thining non-Newtonian. Unsteady boundary conditions were used. In the branch (going up)

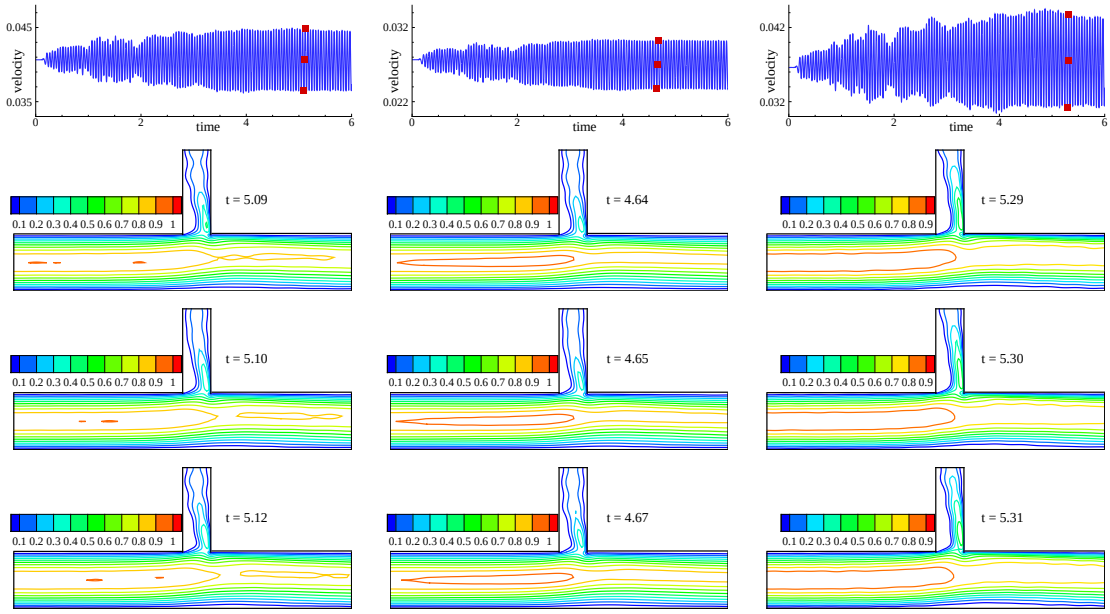

(a) Newtonian (b) shear thickening (c) shear thinning

Figure 5: The graphs of the velocity as the function of time and velocity isolines of unsteady flow of generalized Newtonian fluids by artificial compressibility method (frequency is 20).

the pressure is prescribed by pressure function (20) with considered frequencies f, 2 and 20. In Figure 6 and 7 graphs of velocity as the function of time and the velocity distribution are shown.

As initial data the numerical solution of steady fully developed flow of generalized Newtonian fluid was used. In the Figure 6 the frequency is 2 and in the Figure 7 the frequency is 20.

5. Conclusions

In this paper a finite volume solver for incompressible laminar viscous flows in the branching channel was described. Newtonian model was generalized for generalizing Newtonian fluids flow. Power-law model with different values of power-law index were tested. The explicit Runge-Kutta method was considered for numerical modelling. The convergence history confirms robustness of the applied method. The numerical results obtained by this method were presented and compared.

Two unsteady approaches were considered, the artificial compressibility method and the dual-time stepping method. Both methods were tested for generalized Newtonian fluids with initial data obtained by steady numerical computation.

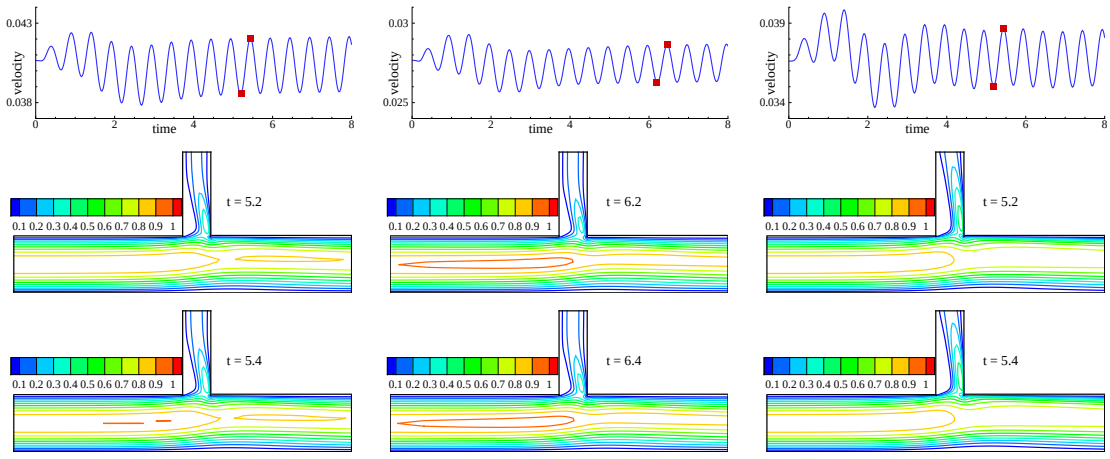

(a) Newtonian (b) shear thickening (c) shear thinning

Figure 6: The graphs of the velocity as the function of the time.

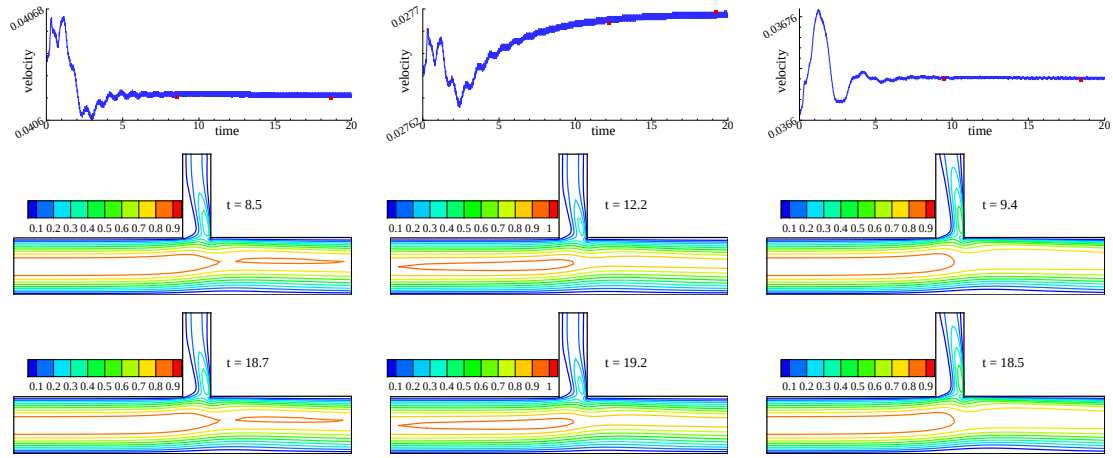

(a) Newtonian (b) shear thickening (c) shear thinning

Figure 7: The graphs of the velocity as the function of the time.

Acknowledgements

This work was partly supported by the grant GACR P201/ 11/1304, GACR 101/09/1539 and GACR 201/08/0012, Research Plan MSM 684 077 0003 and Research Plan MSM 684 077 0010.

References

[1] Chhabra, R. P. and Richardson J. F.: *Non-Newtonian flow in the process industries*. Biddles Ltd, Guildford and King's Lynn, Great Britain, 1999.

[2] Dvořák, R. and Kozel, K.: *Mathematical modelling in aerodynamics (in Czech)*. CTU, Prague, Czech Republic, 1996.

[3] Chorin, A. J.: A numerical method for solving incompressible viscous flow problem. J. Comput. Phys. **135** (1967) 118–125.

[4] Keslerová, R. and Kozel, K.: Numerical simulations of incompressible laminar flow for Newtonian and non-Newtonian fluids. In: K. Kunisch, G. Of, O. Steinbach (Eds), *Numerical Mathematics and Advanced Applications, ENUMATH 2007* (2008) 465–472.

[5] LeVeque, R.: *Finite-volume methods for hyperbolic problems*. Cambridge University Press, 2004.

[6] Gaitonde, A. L.: A dual-time method for two dimensional unsteady incompressible flow calculations. International Journal for Numerical Methods in Engineering **41** (1998) 1153–1166.

[7] Robertson, A. M.: *Review of relevant continuum mechanics*. Birkhäuser Verlag Basel, Switzerland, 2008.

[8] Honzátko, R.: *Numerical simulations of incompressible flows with dynamical and aeroelastic effects*. Ph.D. thesis, Czech Technical University, Prague, Czech Republic, 2007.

[9] Vimmr, J. and Jonášová, A.: Non-Newtonian effects of blood flow in complete coronary and femoral bypasses. Math. Comput. in Simulation **80** (2010) 1324–1336.

[10] Kračmar, S. and Neustupa, J.: Global existence of weak solutions of a nonsteady variational inequality of the Navier–Stokes type with mixed boundary conditions. *Proc. of the International Symposium on Numerical Analysis*, Charles University Prague, (1993) 156–177.

[11] Kračmar, S. and Neustupa, J.: A weak solvability of steady variational inequality of the Navier–Stokes type with mixed boundary conditions. Nonlinear Anal. **47** (2001) 4169–4180.